DESIGN OPTIMIZATION OF COMPENSATION CHICANES IN THE LCLS-II TRANSPORT LINES*

J. Qiang[#], C. E. Mitchell, M. Venturini, LBNL, Berkeley, CA 94720, USA
Y. Ding, P. Emma, Z. Huang, G. Marcus, Y. Nosochkov, T. Raubenheimer, L. Wang, M. Woodley
SLAC, Menlo Park, CA 94025, USA

Abstract

LCLS-II is a 4th-generation high-repetition rate Free Electron Laser (FEL) based x-ray light source to be built at the SLAC National Accelerator Laboratory. To mitigate the microbunching instability, the transport lines from the exit of the linac to the undulators will include a number of weak compensation chicanes with the purpose of cancelling the momentum compaction generated by the main bend magnets of the transport lines. In this paper, we will report on our design optimization study of these compensation chicanes in the presence of both longitudinal and transverse space-charge effects.

INTRODUCTION

The microbunching instability [1-4], seeded by shot noise and driven by collective effects (primarily space-charge), can significantly degrade the quality of the electron beam before it enters the FEL undulators. In our earlier studies, we identified beam transport through the long beamline from the exit of the linac to the entrance of the FELs in the LCLS-II (shown in Figure 1 [5,6]) as
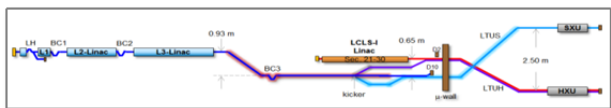

Figure 1: A schematic layout of the LCLS-II.

particularly problematic from the standpoint of the instability. A large instability is observed in the sub-μm range, resulting from the combination of a long (> 2 km) transport line, the presence of several doglegs and other dispersive transport sections, and a relatively low (compared to LCLS) beam energy (4 GeV). To mitigate this effect we proposed [7] to modify the lattice so as to introduce local compensation of the momentum compaction function (R56), thus preventing the longitudinal slippage responsible for the appearance of microbunching. A simple way to realize local compensation is to place weak 4-dipole chicanes (contributing negative R56) next to the main dipoles of the transport line (contributing positive R56). The benefit of these compensation chicanes is demonstrated by the plots of Fig. 2, showing much less current fluctuation after including the compensation chicanes.

The compensation chicanes have been added to the LCLS-II baseline in the October 2015 lattice. Specifically, two compensation chicanes are placed at the two ends of

DL1, the dogleg that takes the beam into the bypass line. The main dispersive sections in the HXR transport line downstream of the spreader consist of two double-bend achromats arranged into a dogleg configuration. Because of space constraints, compensation chicanes are placed next to each of the two dipoles of the second double-bend achromat but only one chicane is used in the first double-bend achromat. In the latter case compensation is not highly localized but was found to be adequate. Similarly, two compensation chicanes are inserted in the SXR transport line.

While the detailed macroparticle simulations, including tracking starting from the injector, confirmed the effectiveness of the compensating chicanes they also indicated that they were not sufficient to eliminate microbunching completely for the nominal setting of laser heating [8]. This is particularly evident in the beam transported to the SXR FEL (see Fig. 2). We found that
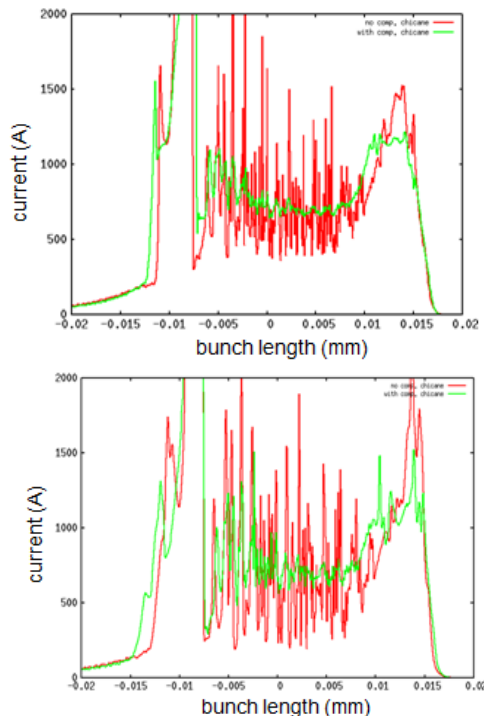

Figure 2: Current profiles at the entrance of the HXR (top) and SXR FEL (bottom) undulators contrasting the lattice with (green) and without (red) compensation chicanes. (Start-to-end simulations of a 100 pC bunch.).

some of the microbunching was due to an interesting 3D effect [9] occurring in the doglegs of the transport line downstream of the Linac. Transverse space-charge fields

in these dispersive regions can induce significant longitudinal slippage and hence contribute to microbunching because of a finite R52 if some energy modulation along the beam is present (e.g. due to microbunching instability developed upstream). Luckily, the direction of the transverse space-charge induced slippage can be countered by R56-induced slippage, opening up the possibility that retuning the compensating chicanes may yield better overall control over the instability compared to exact R56 compensation -- this possibility was recognized in [9]. While we do not have an analytical demonstration yet, the numerical simulations presented here show that indeed there exists an optimal setting for the compensation chicanes for suppression of the instability. The results of these simulations are discussed in the section after the brief description of the computational tools in the following section.

COMPUTATIONAL SETUP

All simulations presented in this study were done using the 3D parallel beam dynamics simulation framework IMPACT [10-12]. It includes a time-dependent 3D space-charge code module IMPACT-T to simulate photo-electron beam generation and acceleration through the photo RF gun, buncher and boosting cavities, and a position-dependent 3D space-charge code module to simulate electron beam transport through the superconducting linac system. Besides the 3D space-charge effects, the simulation also includes coherent synchrotron radiation (CSR) effects through bending magnets, incoherent synchrotron radiation inside each bending magnet, RF cavity structure wakefield, and resistive wall wakefields. All simulations were done using the real number of electrons for three bunch charges, 20 pC, 100 pC, and 300 pC, to capture the initial shot noise of the beam, which can have important impact on the final beam quality and FEL performance due to the microbunching instability.

OPTIMIZATION RESULTS

In the optimization, we scanned the bending angle of all bending magnets in all compensation chicanes by the same percentage factor. The 0 percentage corresponds to the nominal design settings. The core of the final current profile at the entrance of the undulator was fitted by a cubic polynomial. The rms current fluctuation was calculated using the difference between the final core current and the fitted current profile. Figure 3 shows the rms current fluctuation as a function of the percentage of overcompensation for the 100 pC soft x-ray scenario. It is seen that 15-20% increase in the bending angle (corresponding to about a factor of 1.5 overcompensation of R56) yields the least current fluctuation. Figure 4 shows the final longitudinal phase space and current profile with the nominal compensation setting and the 20% overcompensation setting. The 20% over-compensation setting yields much less microbunching fluctuation in both the phase space and the current profile. For the hard x-ray beam line, the 20% overcompensation setting also yields minimum rms fluctuation.

We also optimized the compensation chicanes for the 300 pC scenario. Figure 5 shows the final rms current fluctuation as a function of the overcompensation percentage of the chicane through the soft x-ray beam line. It is seen that the 10-15% overcompensation setting has the least fluctuation. Figure 6 shows the final longitudinal phase space and current profiles with and without 15% overcompensation. Again, 15% over-compensation shows less phase space and current fluctuation compared with the nominal compensation chicane setting. For the hard x-ray beam line, the same 15% overcompensation yields the least current fluctuation.
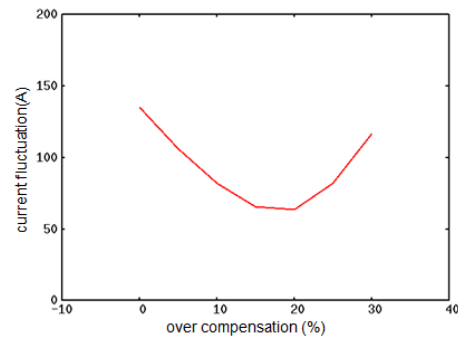

Figure 3: RMS current fluctuation as a function of overcompensation percentage of the compensation chicane setting in the 100 pC soft x-ray scenario.
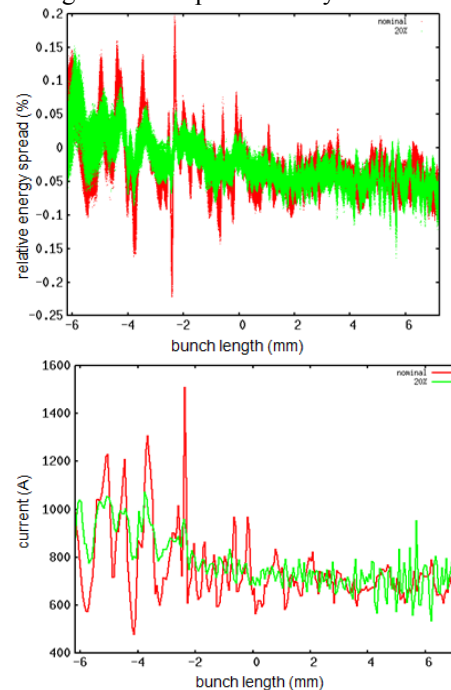

Figure 4: Final longitudinal phase space (top) and current profile (bottom) with nominal (red) and 20% overcompensation (green) settings in the 100 pC soft x-ray scenario.

In the third scenario with 20 pC charge, we performed the same optimization of the compensation chicane strengths. Figure 7 shows the rms final current fluctuation

as a function of overcompensation percentage through the soft x-ray beam line. The 20-30% overcompensation yields the least current fluctuation. Figure 8 shows the final longitudinal phase space and current profile with and without 30% overcompensation. The overcompensated chicane setting has less current fluctuation than the nominal design.
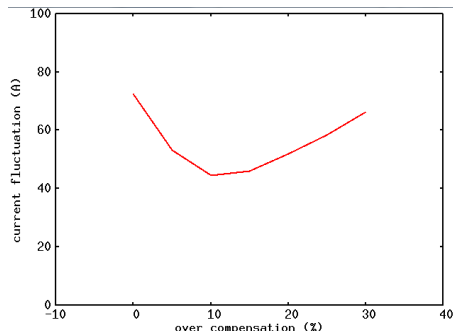

Figure 5: RMS current fluctuation as a function of overcompensation percentage of the compensation chicane setting in the 300 pC soft x-ray scenario.
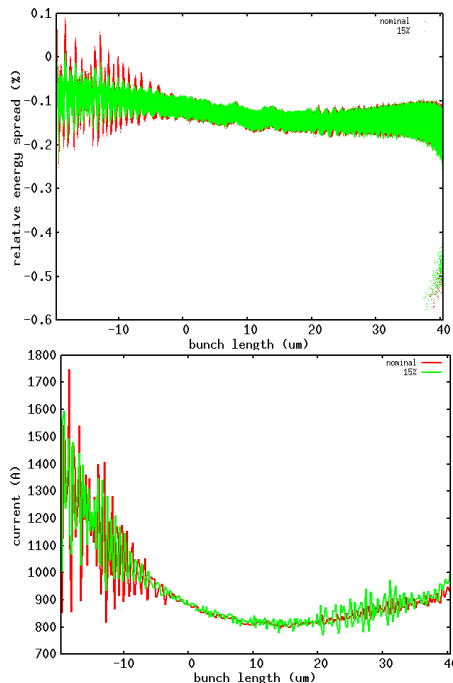

Figure 6: Final longitudinal phase space (top) and current profile (bottom) with nominal (red) and 15% overcompensation settings (green) in the 300 pC soft x-ray scenario.

For the hard x-ray beam line, the 30% overcompensation also yields the minimum rms current fluctuation.

In summary, for the 100 pC scenario, 15–25 % larger bending angle in the compensation chicanes helps reduce the microbunching-induced final current and energy fluctuation significantly. For the 300 pC case, 10–20 % over-compensation helps reduce the final modulation. For the 20 pC case, 15-30 % overcompensation improves the beam current profiles. An interesting question deserving

additional study is whether the number of compensation chicanes could be reduced without affecting their effectiveness. This has not yet been addressed.
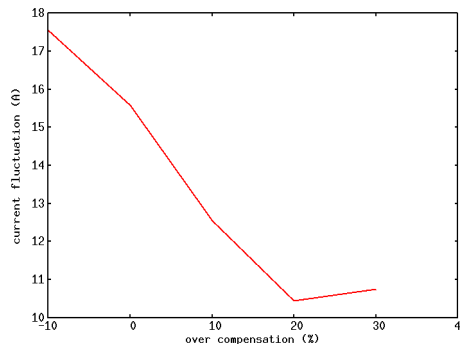

Figure 7: RMS current fluctuation as a function of overcompensation percentage of the compensation chicane setting in the 20 pC soft x-ray scenario.
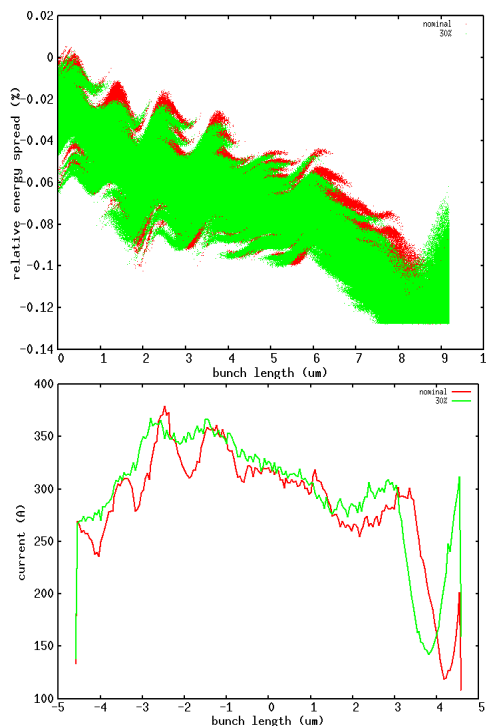

Figure 8: Final longitudinal phase space (top) and current profile (bottom) with nominal (red) and 30% overcompensation settings (green) in the 20 pC soft x-ray scenario.

REFERENCES

[1] M. Borland et al., Nucl. Instrum. Methods Phys. Res., Sect. A 483, 268 (2002).

[2] E. L. Saldin, E. A. Schneidmiller, and M. V. Yurkov, Nucl. Instrum. Methods Phys. Res., Sect. A 483, 516 (2002).

[3] S. Heifets, G. Stupakov, and S. Krinsky, Phys. Rev. ST Accel. Beams 5, 064401 (2002).

[4] Z. Huang and K. J. Kim, Phys. Rev. ST Accel. Beams 5, 074401 (2002).

[5] T. O. Raubenheimer, in proceedings of IPAC2015, Richmond, VA, USA.

[6] P. Emma et al., in proceedings of FEL'14, THP025.

[7] M. Venturini et al., in Proceedings of IPAC2015, p. 1843, Richmond, VA, USA (2015).

[8] M. Venturini, FEL15 Conference, Proceedings (2015).

[9] M. Venturini and J. Qiang, PRST-AB, 18, 054401, (2015).

[10] J. Qiang et al., PRST-AB 9, 044204 (2006).

[11] J. Qiang et al., J. of Comp. Phys., 163, 434 (2000).

[12] J. Qiang et al., PRST-AB 12, 100702 (2009).